CSIRO PUBLISHING
FUNCTIONAL PLANT BIOLOGY

Measuring the diurnal pattern of leaf hyponasty and growth in Arabidopsis – a novel phenotyping approach using laser scanning

Journal:	*Functional Plant Biology*
Manuscript ID:	FP12018.R1
Manuscript Type:	Research paper
Date Submitted by the Author:	n/a
Complete List of Authors:	Dornbusch, Tino; University of Lausanne, Center for Integrative Genomics Lorrain, Séverine; University of Lausanne, Center for Integrative Genomics Kuznetsov, Dmitry; SIB-Swiss Institute of Bioinformatics, University of Lausanne Fortier, Arnaud; SIB-Swiss Institute of Bioinformatics, University of Lausanne Liechti, Robin; University of Lausanne, SIB-Swiss Institute of Bioinformatics Xenarios, Ioannis; SIB-Swiss Institute of Bioinformatics, University of Lausanne Fankhauser, Christian; Center for Integrative Genomics, University of Lausanne
Keyword:	Adaptive response, Arabidopsis spp., Architecture of plants, Diurnal variation, Light quality

Measuring the diurnal pattern of leaf hyponasty and growth in *Arabidopsis* – a novel phenotyping approach using laser scanning

Tino Dornbusch[1], Séverine Lorrain[1], Dmitry Kuznetsov[2], Arnaud Fortier[2], Ioannis Xenarios[2] and Christian Fankhauser[1]

[1]Center for Integrative Genomics, University of Lausanne, 1015 Lausanne, Switzerland

[2]SIB-Swiss Institute of Bioinformatics, University of Lausanne, 1015 Lausanne, Switzerland

Summary (50 to 80 words, three sentences for non Scientists)

Increased leaf elevation angle (hyponasty) and leaf elongation in *Arabidopsis* are caused by different environmental stimuli such as shading by surrounding vegetation. Here we report on a phenotyping approach based on laser scanning to measure the diurnal pattern of these two growth responses. Individual plants can be monitored during several days under different light conditions, with high temporal resolution, in high-throughput and non-invasively.

Abstract (200)

Plants forming a rosette during their juvenile growth phase, such as *Arabidopsis thaliana,* are able to adjust size, position and orientation of their leaves. These growth responses are under the control of the plants circadian clock and follow characteristic diurnal rhythms. For instance, increased leaf elongation and hyponasty -defined here as the increase in leaf elevation angle- can be observed when plants are shaded. Shading is either caused by a decrease in the fluence rate of photosynthetically active radiation (direct shade) or a decrease in the fluence rate of red compared to far-red radiation (neighbor detection).

In this paper we report on a phenotyping approach based on laser scanning to measure the diurnal pattern of leaf hyponasty and increase in rosette radius. In short days, leaves showed a constitutively increased leaf elevation angles compared to long days, but the overall diurnal pattern and the magnitude of up and downward leaf movement was independent of day length. Shade treatment led to elevated leaf angles during the first

day of application, but did not affect the magnitude of up and downward leaf movement in the following day.

Using our phenotyping device, individual plants can be monitored during several days under different light conditions, with low temporal resolution, in high-throughput and non-invasively. It hence represents a proper tool to phenotype light- and circadian clock-mediated growth responses in order to understand the underlying regulatory genetic network.

Key words

Arabidopsis, phenotyping, laser scanning, image processing, hyponasty, petiole angle, leaf elongation, diurnal, circadian clock

Introduction

Being sessile, higher plants need to adapt to their ever-changing environment to optimize primary production and warrant good conditions for their offspring. A way to achieve this is through phenotypic plasticity of the aerial plant body in response to stimuli such as day length, light intensity, solar angle, water/nutrient availability or temperature (de Kroon *et al.* 2009; Novoplansky 2009; Sultan 2010). Adjusting leaf angle is an important aspect of plant plasticity that optimizes the interception of incoming light (Ehleringer 1988) or avoids temperature-related stress (Medina *et al.* 1978).

Plants forming a rosette during their juvenile growth phase, such as *Arabidopsis thaliana,* are able to alter the position, orientation, length, width and shape of their leaves as well. Numerous stimuli can cause these growth responses such as radiation, touch, chemicals, gravity, water or temperature. For instance an upward movement of leaves (referred to as leaf hyponasty), which is the increase in the leaf elevation angle, can be observed in response to submergence (Cox *et al.* 2003; Voesenek *et al.* 2006) or increased temperatures (Koini *et al.* 2009). Hyponasty enables plants to position their leaves above the water surface in case of submergence or to increase transpiration for cooling in case of high temperature. Changes in light quantity, quality or direction can

also trigger leaf movements and increased leaf elongation. *Arabidopsis* leaf blades are usually oriented perpendicular to the incoming light (phototropism). A decrease in the fluence rate of photosynthetic active radiation (E_{PAR}) by direct shading leads to leaf hyponasty and increased petiole elongation (Keller *et al.* 2011) or hypocotyl elongation (Keuskamp *et al.* 2011). This shade avoidance response is not only triggered by a low E_{PAR}, but also by a decrease in the fluence rate of red (R) compared to far-red (FR) light (Mullen *et al.* 2006; Sasidharan *et al.* 2010). The reduced R-FR ratio arises from an increased scattering of FR radiation by surrounding vegetation and thus indicates the presence of neighbor plants, which constitute potential future competitors. Leaf hyponasty and increased petiole elongation in response to low E_{PAR} and low R-FR ratio aim at positioning leaves in the upper part of the canopy, where light conditions are more favorable. In addition to external stimuli, leaf hyponasty and elongation also depend on the internal circadian clock (Millar *et al.* 1995; Salter *et al.* 2003). In *Arabidopsis* grown in regular day-night cycles, leaves move and grow according to a rhythmic diurnal pattern. Leaf growth rate is highest in the early morning and rapidly declines thereafter (Wiese *et al.* 2007). The leaf elevation angle increases during the day followed by a decrease at the end of the night before dawn (Millenaar *et al.* 2005; Mullen *et al.* 2006; Sasidharan *et al.* 2010).

In spite of these dynamic aspects of plant growth, measurements of leaf or petiole elevation angle and length in *Arabidopsis* are quite challenging. Most studies have relied on ruler (Mullen *et al.* 2006), protractor (Keller *et al.* 2011), or photogrammetry (Millenaar *et al.* 2005) as measurement technique. However, plants need to be sampled or illuminated with visible light applying these methods, which perturbs the plants internal circadian clock, and does not allow monitoring of diurnal leaf growth over several days. Our approach based on laser-scanning and infra-red photography allows to over come this obstacle. In addition, laser-scanning as three-dimensional (3D) imaging technique allows to non-destructively measure the whole 3D surface of leaves and opens up exciting possibilities to study architectural traits of different leaves during several days. 3D imaging techniques have already been applied in plant phenotpying, including laser scanning (Kaminuma *et al.* 2004), phase-shifting projected fringe profilometry (Dornbusch *et al.* 2007), X-ray computed tomography (Kaminuma *et al.* 2008; Dhondt *et al.* 2010) or optical projection tomography (Lee *et al.* 2006). The most

advanced approach for *Arabidopsis* phenotyping using these techniques has been developed by Kaminuma *et al.* (2004) who proposed to use laser scanning to extract morphological traits of leaves from measured 3D data. They succeeded in measuring traits such as the orientation of the blade surface and epinasty in a detailed and automated way. Measurements were done on *Arabidopsis* plantlets with two true leaf blades (plus two cotyledons), where leaves were almost horizontally oriented and did not overlap. However, the architecture of *Arabidopsis* plants is usually more complex. Leaves can be oriented more vertically and overlap in later growth stages and are thus not fully captured by the laser scanner. Hence an automated 3D image analysis does not seem applicable. Indeed, to our knowledge, there has been no follow-up work reported using the approach by Kaminuma and co-workers (2004) so far.

Here, we take up the laser scanning approach and propose a phenotyping pipeline using laser scanning and subsequent image analysis. Our goal is to extract traits from these images that can be reliably linked to leaf elevation angle and plant size to measure these growth responses. In this paper, we present our phenotyping pipeline, which includes: i) technical specifications of the ScanAlyzer HTS, ii) plant growth conditions (mainly light and daylength) and iii) and image processing algorithm implemented in Matlab (The MathWorks Inc., Natick, USA). We furthermore give examples of possible applications of our phenotyping method by presenting data on diurnal leaf hyponastic responses caused by different day-length, light intensities (E_{PAR}), light quality (R-FR ratio) and genetic background.

Materials and Methods

Plant growth

The *Arabidopsis thaliana* accession Columbia (Col-0) and the *sav3-2* mutant (Tao *et al.* 2008) were used. Seeds were stratified three days on moist filter paper in the dark at 4°C and sown on a mixture (50:50) of peat-rich soil and vermiculite. Deionized water was added to saturate the growth medium. The soil surface around plants was covered with a thin layer of charcoal to minimize laser reflection. Prior to scanning, plants were kept in a Percival CU-36L4 incubator (Percival Scientific, Inc., Perry, USA) at 21°C for 15 days at long day (16h photoperiod) or 20 days at short day (8h photoperiod). Plants were transferred to the ScanAlyzer HTS 24h before scanning at growth stage 1.05

(Boyes *et al.* 2001) maintaining the entrained photoperiod. The device is Fluorescence tubes were 100 cm above plant level and emitted cool white light (light color 865) at a fluence rate E_{PAR} = 180 µmol m^{-2} s^{-1} in the incubator.

Light conditions

The spectral composition of the light in the ScanAlyzer HTS (Lemnatec GmbH, Würselen, Germany) and the Percival incubator was measured using a USB2000+ UV-VIS spectrometer (Ocean Optics, Inc., Dunedin, USA). For each measurement, 50 spectra were recorded at plant level and different horizontal positions, and averaged to a mean spectrum. The fluence rate of photosynthetically active radiation (E_{PAR}) was computed as the integral from 400nm to 700nm. Likewise, the fluence rate of far-red radiation (E_{FR}) was calculated by integrating the spectrum from 680nm to 760nm (see Supplemental Figure 1). Four different light setups were used in our experiments (Tab. 1). In the ScanAlyzer HTS, E_{PAR} was decreased installing a gray plexiglas filter panel 6 cm underneath the fluorescence tubes. Likewise, E_{FR} was altered switching on the dimmable built-in FR diodes. Different light treatments did neither influence temperature nor humidity inside the measurement chamber due to its large volume (~2 m^3) and high air-exchange rate with the surrounding air-conditioned room (21°C, 70% rel. humidity).

Technical specifications of the ScanAlyzer HTS

Our custom-built version of the Scanalyzer HTS is equipped with fluorescence tubes providing cool white light (light color 865) and dimmable FR diodes (λ = 740 nm). The imaging unit entails a NIR Laser (λ = 905nm, $P \approx 10$ mW) pointing nadir, a camera to record the laser beam Vosskühler CMC-1300 (Allied Vision Technologies GmbH, Stadtroda, Germany) mounted 45° in relation to the laser and a further charged coupled device camera (CCD) camera (Basler scA1400-17gc, Basler AG, Ahrensburg, Germany) mounted nadir to record RGB images (Fig. 1a). The CCD camera is equipped with a ring of near infrared (NIR) diodes (λ = 940nm) around the lens to record images in darkness.

The imaging unit can be programmed to move to specific locations within the measurement chamber approximated 15 cm above plant level. Images can be recorded at a specified times or time-intervals. The measurement space in the ScanAlyzer HTS is divided into 6 slots. Each slot holds a tray containing a maximum of 12 pots (12.3cm-by-7.9cm in size) allowing a maximum imaging capacity is 72 pots. A full scan of 72 pots (laser scan + RGB image) takes approximately 80 minutes. For the data presented here we have usually scanned less 12-36 pots per experiments at a time interval of 40 or 60 minutes.

Conversion of laser scanner images to 3D point clouds

The output of the laser scanner is a 2.5D height-scaled image, 1024-by-1728 pixels in size (Fig. 1b). Each pixel represents a measured point. In the image, the column index (i) is linked to the x-coordinate and the row index (j) to the y-coordinate of a measured point. The RGB color triplet (c) of each pixel encodes its distance from the reference plane (z) and thus represents the z-coordinate of a measured point (Fig. 1b).

In image processing, i and j are normally multiplied with a scale factor to obtain the x and y-coordinate. In our case, images have a perspective distortion caused by the shape of the lens and the focal length. Therefore, each [i, j] doublet has a specific x- and y-coordinate, which are assigned using two distinct look-up tables (matrices). In 2.5D images, the distortion of the x-y plane in the image even depends on z. Therefore we need to assign an x- and an y-coordinates to each [i, j, c] triplet. The corresponding look-up tables Kx and Ky are hence 3D matrices (see Supplemental Material).

To obtain Kx and Ky, a black panel (12.3cm-by-7.9cm) with a rectangular grid (1cm spaced and 1mm wide grid lines) was scanned at seven positions (0cm $\leq z \leq$ 6.58cm). Intersections of grid lines in all seven scanned images were manually selected. Thus for 672 [i, j, c] triplets we obtained a x-coordinate and a y-coordinate, respectively, which yielded a sparse matrix for Kx and Ky. The full matrices were computed by linear interpolation. Scanning the grid at each z, we obtained seven mean values for the color index c and the corresponding z-coordinate. These values were used to fit a second order polynomial to obtain a look-up table, in which for each c is related to z.

The maximum dimensions of the calibrated measurement space are 13.56cm x 8.92cm x 6.58cm. The described algorithm was implemented in Matlab R2009b (MathWorks

Inc., Natick, USA). Source code to convert images to point clouds, the matrices *Kx* and *Ky* and a sample image (Fig. 1b) are given in the Supplemental material.

Test of image conversion

First, we tested whether the proposed image conversion of pixel coordinates in 2.5D height-scaled images (i, j, c) to Carthesian coordinates (x, y, z) was precise enough. To do this, we scanned a panel of 23 circles at five different heights (z) and three different inclination angles (Fig. 2a,b). Circles had a predefined area ($0.0020\text{cm}^2 \leq A_{org} \leq 3.46\text{cm}^2$). Background discrimination in binary images was done by choosing a gray threshold of 2 ($0 \leq \text{gray} \leq 255$). Hence all pixels with gray>0 are belong to measured circles. In the following cluster analysis (Matlab function bwlabel), 23 clusters of interconnected pixels were detected, each corresponding to a scanned circle. Boundary pixels for each cluster were identified and pixel coordinates transformed to Cartesian coordinates using the matrices *Kx* and *Ky*. Points computed this way were connected to triangles using Delaunay triangulation.

The sum of the triangle area corresponded to the measured area of the circle A_{scan}. Comparing measured circle area A_{scan} to predefined values A_{org} allows to demonstrate the precision of our image conversion. For circles scanned at different height or inclination (Fig. 4c), values for A_{scan} deviated little from A_{org} with a minor overestimation of A_{scan}. All points fell close to the optimal 1:1 line. The mean relative error (MRE) was 0.094 was relatively, which could be attributed to the improper area estimation of very small circles. For circles with a size similar to *Arabidopsis* leaves (A > 0.5 cm^2), the MRE was 0.038.

Processing of 3D point clouds

First, we segmented the whole measured point cloud (PC) into m subsets PC_{plant} that include all points measured for each plant. First we selected P_0 for each plant, which is geometrically the position of the shoot apical meristem (Fig. 3a). For time-lapse images, the selection of P_0 was done once per day for each plant at zeitgeber time t =[3, 27, 51]. For PCs measured in between two manual selections (*e.g.* $3 > t > 27$), P_0 was computed using linear interpolation. Next, P_0 was subtracted from PC, shifting the origin of the coordinate system of PC to P_0. Points were assigned to PC_{plant}, which had a distance $r \leq$

1.8cm to P_0 and z > -0.1cm (see Fig. 3a). In our experiment leaves were always shorter than the chosen value for r (Fig. 3d).

The distribution of the spherical coordinates azimuth angle (θ), elevation angle (φ) and radius (r) of PC_{plant} is given in Fig 3c-d. They are related to plant traits as follows: θ = phylotaxis, φ =leaf elevation angle and r = rosette radius.

Data processing

For the data presented here we used mean values for φ_{mean} and r_{mean} of all points in PC_{plant}. Since we recorded time-lapse images of individual plants, we can also display time-courses $\varphi_{mean}(t)$ and $r_{mean}(t)$ illustrated in Figure 4 as:

$$\phi_{mean}(t) = \frac{1}{n_{plant}} \sum_{n=1}^{n_{plant}} \phi_{mean}(t,n) \qquad \text{Eq.1}$$

$$r_{mean}(t) = \frac{1}{n_{plant}} \sum_{n=1}^{n_{plant}} r_{mean}(t,n) \qquad \text{Eq.2}$$

where t is the zeitgeber time and n_{plant} is the total number of measured plants. Hence values for φ_{mean} and r_{mean} measured for 15-30 individual plants were averaged at a given time t.

We further aggregate $\varphi_{mean}(t)$ was used to compute:

$$\Delta\phi_{mean} = \frac{1}{n_{plant}} \left(\sum_{n=1}^{n_{plant}} \phi_{mean}(t_{max},n) - \sum_{n=1}^{n_{plant}} \phi_{mean}(t_{min},n) \right), \qquad \text{Eq.3}$$

where $\Delta\varphi_{mean}$ is the daily amplitude of leaf movement (Fig. 4), t_{max} is the time during the 24h period, where leaves show the steepest elevation angle (around dusk) and t_{min} is the time during the 24h period, where leaves show the lowest elevation angle (usually 3h after dawn). Likewise, for $r_{mean}(t)$ we applied:

$$\Delta r_{\text{mean}} = \frac{1}{n_{\text{plant}}}\left(\sum_{n=1}^{n_{\text{plant}}} r_{\text{mean}}(27,n) - \sum_{n=1}^{n_{\text{plant}}} r_{\text{mean}}(3,n)\right), \qquad \text{Eq.4}$$

where Δr_{mean} represents a measure for the daily increase in rosette radius (Fig. 4). The non-parametric Wilcoxon Rank-Sum Test was used to test differences of measured traits between treatments, where small *P*-values indicate that independent samples follow continuous distributions with different medians.

Results

Diurnal pattern of φ_{mean} for the different treatments

In the following section we provide examples for leaf hyponasty in *Arabidopsis* for different light conditions and genotypes using our phenotyping approach. The analysis of time-lapse images yielded φ_{mean} as a function of zeitgeber time t measured in hours $\varphi_{\text{mean}}(t)$ (Eq. 3; see Fig. 5). Leaves moved up (increase in leaf elevation angle) during the day and moved down during the night approaching a minimum elevation angle 2-3h after dawn. An unexpected abrupt upward movement of leaves was observed under high E_{PAR} and long day conditions, immediately after switching off the light (Fig. 5a). This phenomenon was observed throughout all experiments under these conditions (data not shown).

In short days, leaves showed a constitutively increased φ_{mean} compared to long day conditions (Fig. 5a). Plants were already entrained in the respective photoperiod prior to measurements and had already elevated leaves in short days upon transfer to the phenotyping device. Surprisingly, $\varphi_{\text{mean}}(t)$ were virtually parallel for long and short day, indicating that the overall diurnal pattern of up and downward leaf movement was independent of day length (Fig. 5a). Moreover, the amplitude of leaf movement $\Delta\varphi_{\text{mean}}$ was not different between both treatments in the two days (Fig. 5d, Column I,II, P=0.022).

Next, we investigated how shade treatments using low E_{PAR} or high E_{FR} affected the pattern of $\varphi_{\text{mean}}(t)$. Both led to increased values for φ_{mean} during the first hours ($3 < t < 16$; Fig. 5b), whereas the kinetics differed between the two treatments. Hyponastic movement of leaves started right after the shade treatment had been initiated at $t = 3$.

The amplitude of leaf movement $\Delta\varphi_{mean}$ was increased upon shade treatments compared to the control during the first day (Fig. 5d; Column II-IV, $P<0.001$). After the phase of downward movement (night and early morning), at $t = 27$ leaves did not return to the initial elevation angle, which they had previously adopted at $t = 3$ the day before. During the second day, $\Delta\varphi_{mean}(t)$ followed the typical diurnal pattern, but values for φ_{mean} remained constitutively increased (Fig. 5b). Compared to the control, estimated values for $\Delta\varphi_{mean}$ were bigger at high E_{FR} (Fig. 5d; Column II,III, $P<0.001$), but the same for E_{PAR} (Fig. 5d; Column II,IV, $P=0.812$).

Lastly, we compared the response of the *sav3-2* mutant, affected in shade-induced (low E_{PAR}) hyponasty, compared to Col-0 under low E_{PAR} (Fig. 5c). Initial values for φ_{mean} at $t=3$ were the same magnitude for both genotypes. In the *sav3-2* mutant, φ_{mean} did not increase to the same extent as for the Col-0 control after shade treatment using low E_{PAR} (Fig. 5c). This decreased response is also expressed in smaller values for $\Delta\varphi_{mean}$ in both days measured (Fig. 5d, Column IV-V, $P<0.001$). Thus, hyponastic response of leaves to low E_{PAR} was impaired but not completely absent in the *sav3-2* mutant.

Diurnal pattern of r_{mean} for the different treatments

The second trait we have measured is r_{mean} for the different light conditions and genotypes. The apparent increase in r_{mean} (Fig. 6) during the day coincides with the increase in φ_{mean} and is a measurement artifact, which is discussed below. To compare between treatments we only used values for r_{mean} are given for zeitgeber time $t=3$, 27, 51 (highlighted as open circles in Fig. 6), where leaves were at their most horizontal position. These values were used to compute Δr_{mean} (Eq. 4).

Values for r_{mean} were smaller in short days compared to long days at the beginning of measurements at t=3 (Fig. 6a) and the difference between the two treatments increased towards t=51. Likewise, values for Δr_{mean} were smaller in short day compared to long day (Fig. 6d, Column I-II, $P<0.001$), which in turn indicates a decreased leaf elongation in response in short day compared to long day conditions.

Shade treatment using low E_{PAR} had no impact on the magnitude of r_{mean} (Fig. 6b). Differences in Δr_{mean} were not significant ($P>0.01$). Shade treatment using high E_{FR} led

to increased values for r_{mean} at t=27 and t=51 compared to control (Fig. 6b). However, Δr_{mean} during the first day was significantly increased compared to the control (Fig. 6d, Column II-III, P<0.001).

Furthermore, a clear phenotype regarding r_{mean} was observed for the *sav3-2* mutant, which had smaller values for r_{mean} (Fig. 6c) and for Δr_{mean} compared to Col-0 control (Column IV-V, P<0.001). This indicates that leaf elongation was impaired in the same way as leaf hyponasty in the *sav3-2* mutant compared to Col-0 under the investigated conditions. Our phenotyping approach is able to quantify this effect.

Discussion

We are interested in studying light-mediated growth responses in *Arabidopsis* and understanding the underlying regulatory cellular and molecular processes. Previous work has mainly focused on hypocotyl length as a phenotypic marker, but other traits such as light-mediated leaf hyponasty or elongation have received less attention (Millenaar *et al.* 2005; Mullen *et al.* 2006; Lorrain *et al.* 2008; Sasidharan *et al.* 2010; Keller *et al.* 2011; Keuskamp *et al.* 2011; Polko *et al.* 2012). Our phenotyping method based on laser scanning provides a non-invasive tool to measure the diurnal kinetics of leaf hyponasty with high-throughput and high temporal resolution (<1h). Individual plants can be subjected to two distinct fluence rates of PAR and different R/FR ratios (Tab. 1). Entrained day-night cycles can be maintained, which allows monitoring of plants during several days.

In this paper, we provide an initial characterization of our phenotyping device and the developed image processing pipeline. The principal outputs of our method are time-courses of two traits: i) $\varphi_{mean}(t)$ -a marker for leaf hyponasty- and ii) $r_{mean}(t)$ -a marker for rosette radius or average leaf length. Both traits have been measured at a temporal resolution of less than or equal to 1h during several days in *Arabidopsis* in an early growth stage 1.05 (Boyes *et al.* 2001), where leaf length was usually smaller than 1.8 cm. This way 5-6 plants could be grown in one pot without overlapping of leaves between plants. The maximum leaf length of plants is 3.9 cm to be entirely scanned. In this case only two plants per pot can be scanned. The plant size limitation is clearly a disadvantage of our approach, since care need to be taken that leaves of neighboring plants do not overlap within the filter radius (here 1.8 cm) specified in the image

analysis. In case of overlapping measured points from neighboring plants perturb the measurements.

The geometric assembly of the laser scanner is optimized to measure horizontally oriented leaves (Fig. 1a). However, leaf hyponasty leads to a situation, such that only the upper part of leaves can be measured. In this case, certain parts of the plant are masked by leaves and are therefore not visible to the camera or not lit by the laser. This does not affect the correct assessment φ_{mean}, since leaves are relatively straight, but the correct assessment of r_{mean} (Fig. 6) The apparent increase in r_{mean} -as leaves move up- is caused by the incapacity of the laser scanner to record the lower parts of leaves (with small values for r) at high leaf elevation angles. To compare between treatments, we therefore only used values r_{mean} 3h after dawn to compute Δr_{mean} (Eq. 4), when leaves were oriented most horizontally, which was the optimal position for scanning.

Another potential application for our plant phenotyping method is the measurement of architectural traits for individual leaves, such as petiole angle or leaf blade area. Assuming the ideal case, where the complete leaf surface can be scanned and converted into a 3D point cloud, automated surface triangulation can be applied as proposed by Kaminuma *et al.* (2004). The resulting 3D surface could then be analyzed to directly derive the traits of interest. In experimental conditions, leaves overlap or obscure certain parts of the plant rendering the measured plant surface incomplete (see Fig. 4a and 3D data in Supplemental material). To overcome this obstacle, a model based reconstruction of individual leaf architecture could be applied as has been already proposed for cereal leaves (Dornbusch *et al.* 2007).

Presented data on *Arabidopsis* leaf hyponasty in response to different shade treatments agrees with data obtained in similar studies. High E_{FR} or low E_{PAR} leads to leaf hyponasty starting shortly after the application of the shade treatment (Mullen *et al.* 2006; Millenaar *et al.* 2009; Sasidharan *et al.* 2010; van Zanten *et al.* 2010) and the *sav3-2* mutant is impaired in this shade-avoidance response (Tao *et al.* 2008; Moreno *et al.* 2009; Keller *et al.* 2011). However, these studies usually have measured the leaf responses to shade during one day and constant light, or at a single time point.

According to our data, the diurnal magnitude of up- and down leaf movement follows the pattern of the control in the second day after the shade treatment, except that leaves remain constitutively elevated (Fig. 5).

Mullen *et al.* (2006) made measurements of the diurnal pattern of leaf hyponasty in 12h day-night cycles, which looks very similar to our data. They also show an abrupt upward movement of leaves immediately after switching off the light (Fig. 5a). However the underlying mechanisms have not been discussed. A mutant screen could help to identify genes involved in this growth response. It seems that long days (≥ 12h) and high E_{PAR} promote this effect, whereas short day and/or low E_{PAR} inhibit it.
To our knowledge, hyponastic movements of single leaves have not been measured following several days. Thus it is not known how long leaves do follow diurnal up- and down movements and whether cell elongation in the petiole is a prerequisite. These questions could be addressed with our phenotyping method.
Wiese *et al.* (2007) have measured the diurnal pattern of leaf growth in *Arabidopsis* in 12h day-night cycles. They show a peak growth rate shortly after dawn, which coincides with the phase of rapid downward movement of leaves in our data (Fig. 5). There is thus a correlation between the rapid downward movement of leaves and increased leaf growth. This leads to the unanswered question of whether the regulation of leaf hyponasty and elongation rely on the same genetic regulatory network. On the one hand, leaf hyponasty is mainly driven by differential cell elongation between the abaxial and adaxial epidermis cells at the very base of the petiole (Polko *et al.* 2012). On the other hand, petiole growth by cell proliferation and elongation is biggest towards the blade-petiole junction (Ichihashi *et al.* 2011). Thus both growth processes are spatially separated. One may further speculate that the regulatory mechanisms leading to leaf hyponasty and elongation are somewhat different because of this spatial separation. We would like to address this issue in future work and apply the phenotyping method that has been presented in this paper.

Acknowledgements
The University of Lausanne and the Swiss SystemX.ch project (‘SyBIT’ and ‘Plant Growth in a Changing Environment’) funded this work. T. Dornbusch benefitted from a Marie Curie Intra-European Fellowships (No. 275999). We thank the Department of Molecular Plant Biology for the access to their plant facilities. Joanne Chory provided the *sav3-2* seeds.

References

Boyes, DC, Zayed, AM, Ascenzi, R, McCaskill, AJ, Hoffman, NE, Davis, KR, Görlach, J (2001) Growth stage-based phenotypic analysis of Arabidopsis: a model for high throughput functional genomics in plants. *Plant Cell* **13**, 1499-1510.

Cox, MCH, Millenaar, FF, Van Berkel, YEMdJ, Peeters, AJM, Voesenek, LACJ (2003) Plant movement. Submergence-induced petiole elongation in Rumex palustris depends on hyponastic growth. *Plant Physiology* **132**, 282-291.

de Kroon, H, Visser, EJW, Huber, H, Mommer, L, Hutchings, MJ (2009) A modular concept of plant foraging behaviour: the interplay between local responses and systemic control. *Plant, Cell & Environment* **32**, 704-712.

Dhondt, S, Vanhaeren, H, Van Loo, D, Cnudde, V, Inzé, D (2010) Plant structure visualization by high-resolution X-ray computed tomography. *Trends in Plant Science* **15**, 419-422.

Dornbusch, T, Wernecke, P, Diepenbrock, W (2007) A method to extract morphological traits of plant organs from 3D point clouds as a database for an architectural plant model. *Ecological Modelling* **200**, 119-129.

Ehleringer, JR (1988) Changes in leaf characteristics of species along elevational gradients in the Wasatch Front, Utah. *American Journal of Botany* **75**, 680-689.

Ichihashi, Y, Kawade, K, Usami, T, Horiguchi, G, Takahashi, T, Tsukaya, H (2011) Key Proliferative Activity in the Junction between the Leaf Blade and Leaf Petiole of Arabidopsis. *Plant Physiol* **157**, 1151-1162.

Kaminuma, E, Heida, N, Tsumoto, Y, Yamamoto, N, Goto, N, Okamoto, N, Konagaya, A, Matsui, M, Toyoda, T (2004) Automatic quantification of morphological traits via three-dimensional measurement of Arabidopsis. *The Plant Journal* **38**, 358-365.

Kaminuma, E, Yoshizumi, T, Wada, T, Matsui, M, Toyoda, T (2008) Quantitative analysis of heterogeneous spatial distribution of Arabidopsis leaf trichomes using micro X-ray computed tomography. *The Plant Journal* **56**, 470-482.

Keller, MM, Jaillais, Y, Pedmale, UV, Moreno, JE, Chory, J, Ballaré, CL (2011) Cryptochrome 1 and phytochrome B control shade-avoidance responses in Arabidopsis via partially independent hormonal cascades. *The Plant Journal* **67**, 195-207.

Keuskamp, DH, Sasidharan, R, Vos, I, Peeters, AJM, Voesenek, LACJ, Pierik, R (2011) Blue light-mediated shade avoidance requires combined auxin and brassinosteroid action in Arabidopsis seedlings. *The Plant Journal* **67**, 208-217.

Koini, MA, Alvey, L, Allen, T, Tilley, CA, Harberd, NP, Whitelam, GC, Franklin, KA (2009) High Temperature-Medated Adaptations in Plant Architecture Require the bHLH Transcription Factor PIF4. *Current Biology* **19**, 408-413.

Lee, K, Avondo, J, Morrison, H, Blot, L, Stark, M, Sharpe, J, Bangham, A, Coen, E (2006) Visualizing plant development and gene expression in three dimensions using optical projection tomography. *Plant Cell* **18**, 2145-2156.

Lorrain, S, Allen, T, Duek, PD, Whitelam, GC, Fankhauser, C (2008) Phytochrome-mediated inhibition of shade avoidance involves degradation of growth-promoting bHLH transcription factors. *The Plant Journal* **53**, 312-323.

Medina, E, Sobrado, M, Herrera, R (1978) Significance of leaf orientation for leaf temperature in an Amazonian sclerophyll vegetation. *Radiation and Environmental Biophysics* **15**, 131-140.

Millar, AJ, Straume, M, Chory, J, Chua, NH, Kay, SA (1995) The regulation of circadian period by phototransduction pathways in Arabidopsis. *Science* **267**, 1163-1166.

Millenaar, F, Cox, M, van Berkel, Y (2005) Ethylene-induced differential growth of petioles in Arabidopsis. Analyzing natural variation, response kinetics, and regulation. *Plant Physiology* **137**, 998-1008.

Millenaar, F, van Zanten, M, Cox, M (2009) Differential petiole growth in Arabidopsis thaliana: photocontrol and hormonal regulation. *New Phytologist* **184**, 141-152.

Moreno, JE, Tao, Y, Chory, J, Ballaré, CL (2009) Ecological modulation of plant defense via phytochrome control of jasmonate sensitivity. *PNAS* **106**, 4935-4940.

Mullen, JL, Weinig, C, Hangarter, RP (2006) Shade avoidance and the regulation of leaf inclination in Arabidopsis. *Plant, Cell & Environment* **29**, 1099-106.

Novoplansky, A (2009) Picking battles wisely: plant behaviour under competition. *Plant, Cell & Environment* **32**, 726-41.

Polko, JK, van Zanten, M, van Rooij, JA, Marée, AFM, Voesenek, LACJ, Peeters, AJM, Pierik, R (2012) Ethylene-induced differential petiole growth in Arabidopsis thaliana involves local microtubule reorientation and cell expansion. *New Phytol* **193**, 339-348.

Salter, MG, Franklin, KA, Whitelam, GC (2003) Gating of the rapid shade-avoidance response by the circadian clock in plants. *Nature* **426**, 680-683.

Sasidharan, R, Chinnappa, CC, Staal, M, Elzenga, JTM, Yokoyama, R, Nishitani, K, Voesenek, LACJ, Pierik, R (2010) Light quality-mediated petiole elongation in Arabidopsis during shade avoidance involves cell wall modification by Xyloglucan Endotransglucosylase/Hydrolases. *Plant Physiology* **154**, 978-990.

Sultan, SE (2010) Plant developmental responses to the environment: eco-devo insights. *Current Opinion in Plant Biology* **13**, 96-101.

Tao, Y, Ferrer, J-L, Ljung, K, Pojer, F, Hong, F, Long, JA, Li, L, Moreno, JE, Bowman, E, Ivans, LJ, Cheng, Y, Lim, J, Zhao, Y, Ballaré, CL, Sandberg, G, Noel, JP, Chory, J (2008) Rapid synthesis of auxin via a new tryptophan-dependent pathway is required for shade avoidance in plants. *Cell* **133**, 164-176.

van Zanten, M, Pons, T, Janssen, J (2010) On the relevance and control of leaf angle. *Critical Reviews in Plant Sciences* **29**, 300-316.

Voesenek, LACJ, Colmer, TD, Pierik, R, Millenaar, FF, Peeters, AJM (2006) How plants cope with complete submergence. *New Phytologist* **170**, 213-226.

Wiese, A, Christ, MM, Virnich, O, Schurr, U, Walter, A (2007) Spatio-temporal leaf growth patterns of Arabidopsis thaliana and evidence for sugar control of the diel leaf growth cycle. *New Phytologist* **174**, 752-761.

Tab. 1: The four light setups (I-IV) adjustable in our phenotyping device characterized by mean values (standard deviation) of the fluence rate of photosynthetically active radiation (E_{PAR}) or far-red radiation (E_{FR}) for each setup Arrows indicate high (↑ or low (↓ E_{PAR} and E_{FR}, respectively. Red color highlights deviation of light setup from control conditions.

Light setup	E_{PAR} (µmol m^{-2} s^{-1})	E_{FR} (µmol m^{-2} s^{-1})
I. ↑E_{PAR} ↓E_{FR}	150 (10)	4.5 (0.3)
II. ↑ E_{PAR} ↑E_{FR}	150 (10)	7.5 (0.3) to 150 (10)
III. ↓ E_{PAR} ↓E_{FR}	35 (3)	1.5 (0.2)
IV. ↓ E_{PAR} ↑E_{FR}	35 (3)	2.5 (0.3) to 50 (4)

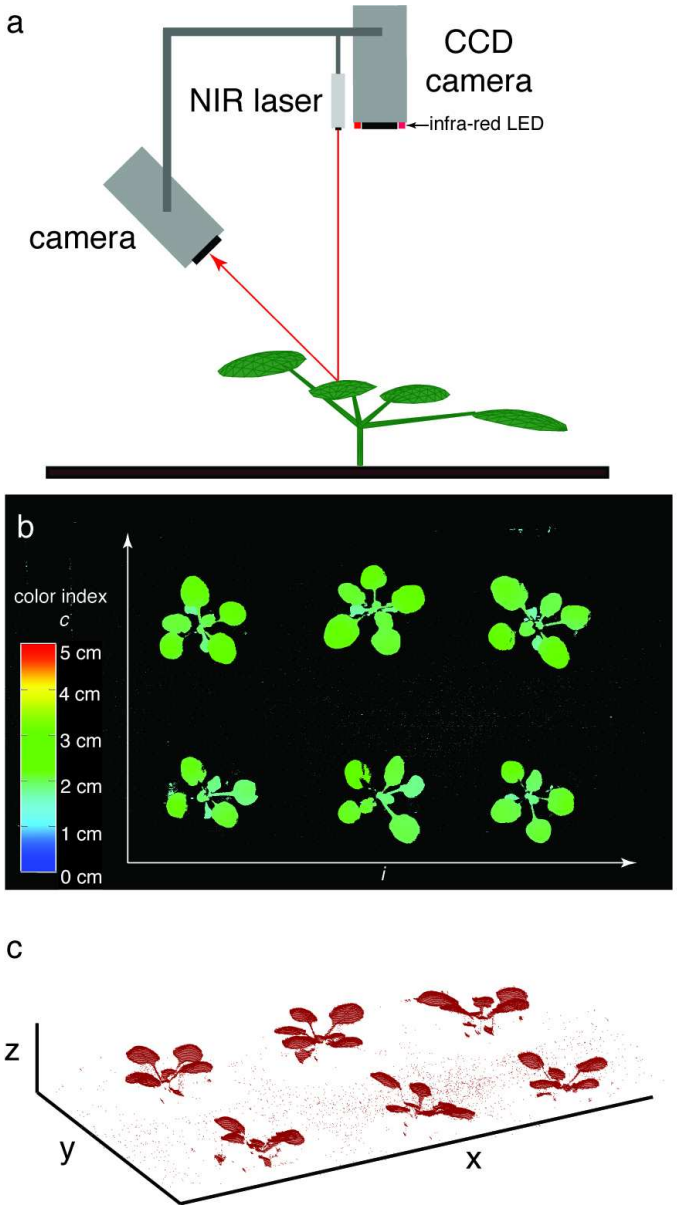

Fig. 1: (a) Laser scanner and charged coupled device (CCD) camera mounted on the imaging unit in the Scanalyzer HTS phenotyping device; (b) 2.5D height scaled image (1024-by-1728 pixels) containing six Arabidopsis plants (image provided as Supplemental Material). For a better visualization, the color in (b) was adjusted compared to the recorded original image. (c) 3D point cloud computed from the recorded 2.5D image using our developed image conversion. The Matlab script and required data for image conversion are available in the Supplemental material.
320x548mm (72 x 72 DPI)

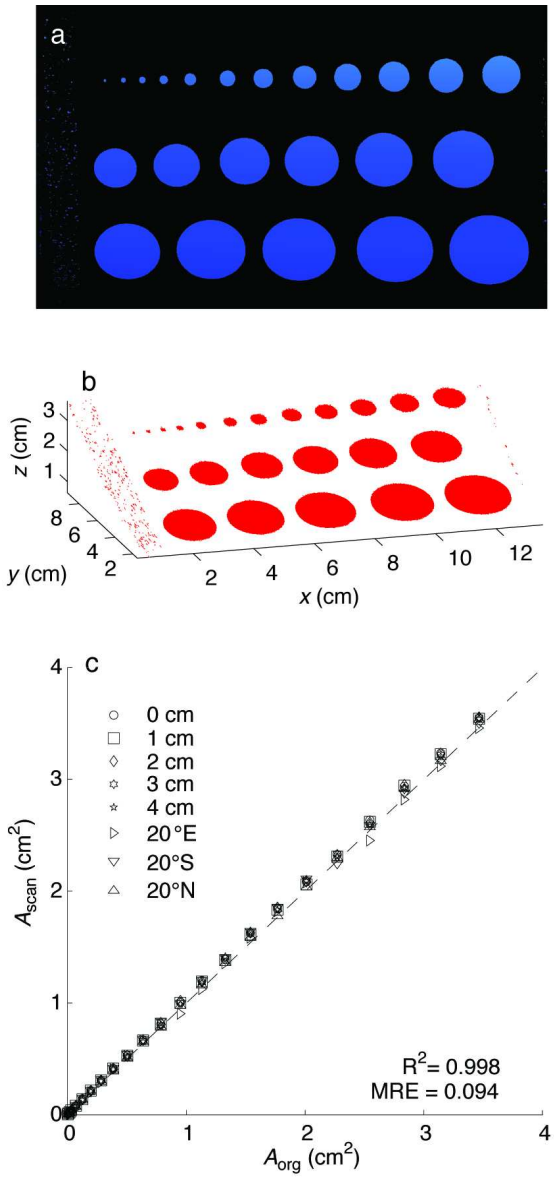

Fig. 2: (a) Panel with 23 circles scanned with the ScanAlyzer HTS at an angle of 20°, (b) point cloud representing these circles in 3D after image conversion, (c) circle area computed from measured 3D points Ascan vs. predefined circle area Aorg on the panel. The dashed line is the 1:1 line. Values for the coefficient of determination (R2) and mean relative error (MRE) are given.
332x642mm (72 x 72 DPI)

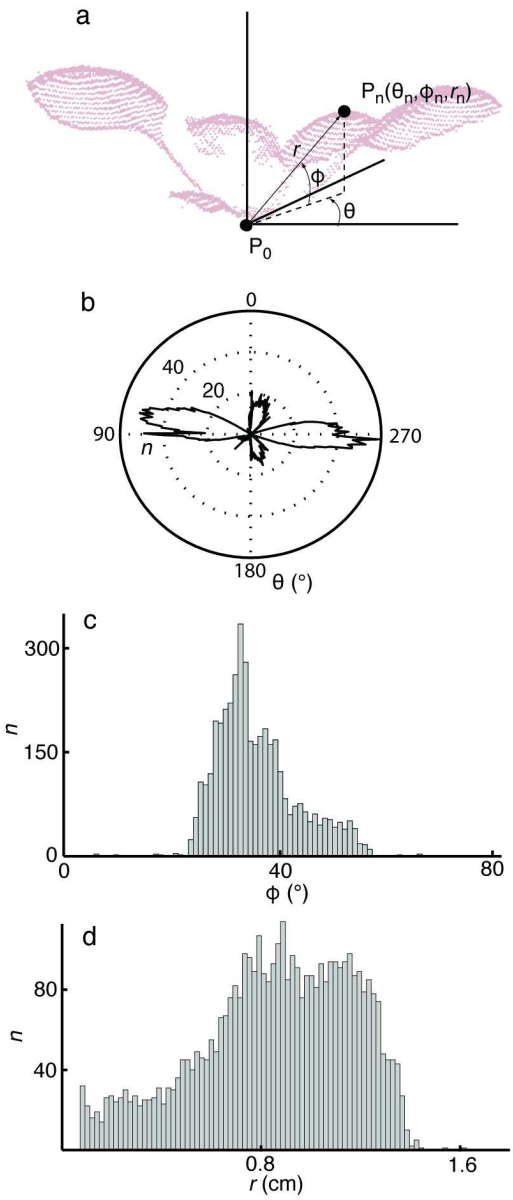

Fig. 3: (a) Measured 3D point cloud of an Arabipopsis plant (PCplant); P0 = selected basal plant point, which coincides with the position of the shoot apical meristem of that plant; Pn = sample point to illustrate the definition of its spherical coordinates (θn, φn, rn); (b-d) Histograms illustrating the distribution of θ, φ and r for points in PCplant given in (a): b) θ vs. n, c) φ vs. n , d) r vs. n; where n = number of points per bin.
305x661mm (72 x 72 DPI)

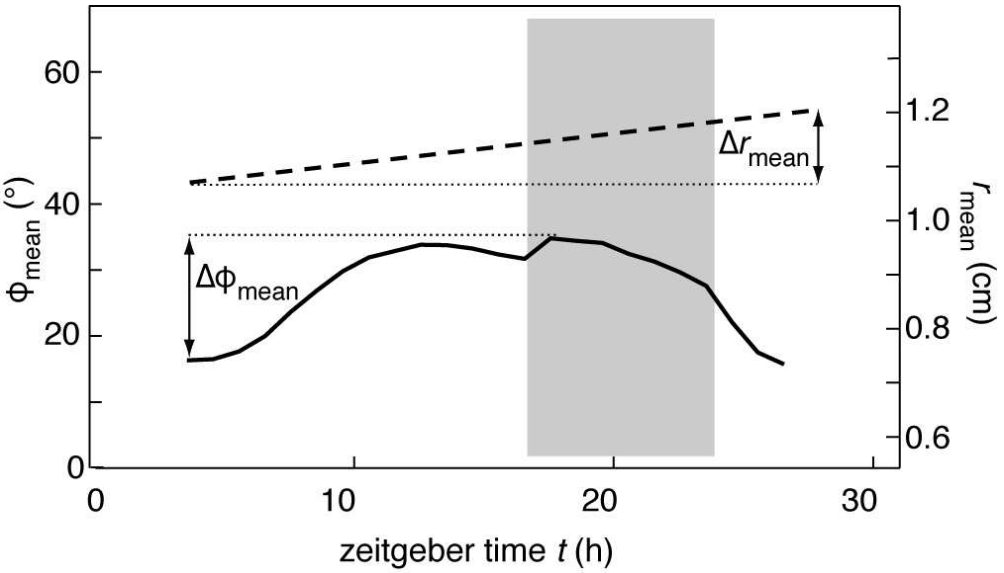

Fig. 4: Diurnal pattern of the φmean(t) -a marker for mean elevation angle- as solid line and rmean(t) – a marker for mean rosette radius- as dashed line. The gray box indicates the entrained night period, which was maintained during measurements. Δφmean as the measure for the daily amplitude of leaf movement; Δrmean as the measure for the daily increase in rosette radius.
357x204mm (72 x 72 DPI)

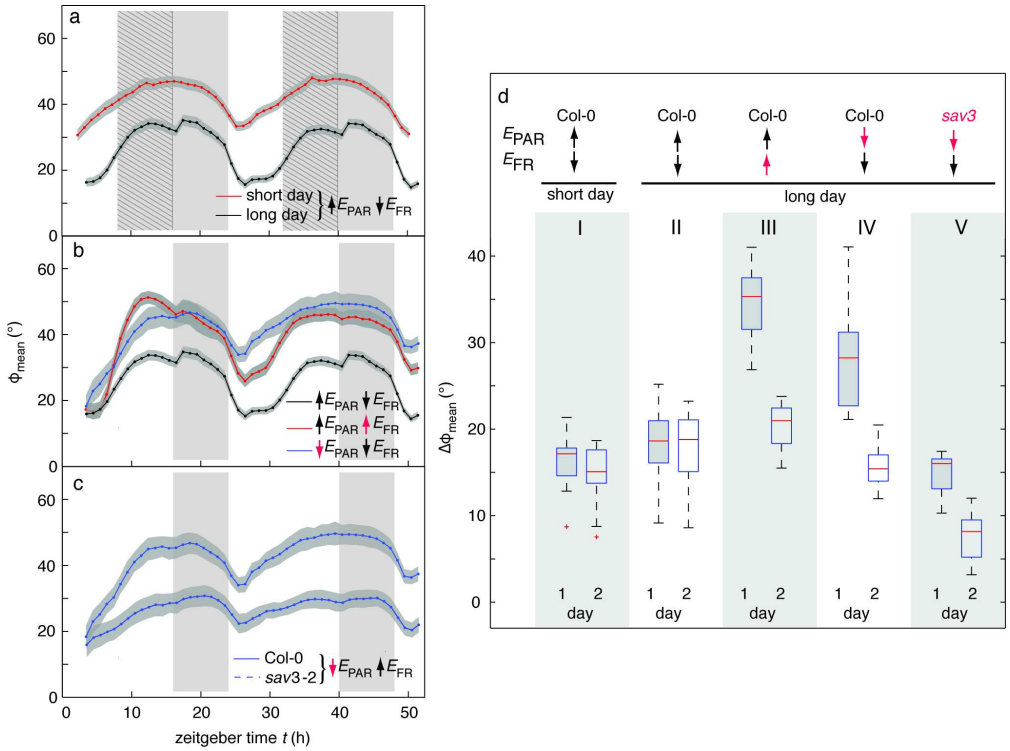

Fig. 5: (a-c) Diurnal pattern of φmean as a marker the mean elevation angle of plants. Dots represent mean values for φmean computed from 15-30 individual plants. The grayish band around mean values for φmean represent the 95% confidence interval of mean estimate. Vertical gray boxes indicate the entrained night period in long day and the hatched part the supplemental night time in short day conditions. Plants were grown in a separate incubator at 21°C, EPAR=180 µmol m-2 s-1 and photoperiod for 15 days (long day) or 20 days (short day) prior to measurements. Specific treatments: (a) black line: long day; red line: short day; for both treatments: Col-0 at normal EPAR=150 µmol m-2 s-1 and normal EFR =4.5 µmol m-2 s-1; (b) black line: normal EPAR=150 µmol m-2 s-1, EFR =4.5 µmol m-2 s-1; red line: normal EPAR=150 µmol m-2 s-1 and supplemental EFR =22.5 µmol m-2 s-1; blue line: reduced EPAR=39 µmol m-2 s-1; reduced EFR =1.5 µmol m-2 s-1); (c) solid line: Col-0; dashed line: sav3-2 mutant; reduced EPAR=39 µmol m-2 s-1; EFR =1.5 µmol m-2 s-1; (d) boxplots of the daily amplitude of leaf movement Δφmean measured for two consecutive days for different treatments presented in (a-c); from left to right: (I) Col-0, EPAR=150 µmol m-2, EFR =4.5 µmol m-2 s-1, short day; (II) Col-0, EPAR=150 µmol m-2, EFR =4.5 µmol m-2 s-1, long day, (III) Col-0, EPAR=150 µmol m-2, EFR =22.5 µmol m-2 s-1, long day; (IV) Col-0, EPAR=39 µmol m-2 s-1; EFR =1.5 µmol m-2 s-1, long day, (V) sav3-2 mutant; EPAR=39 µmol m-2 s-1; EFR =1.5 µmol m-2 s-1, long day.
724x539mm (72 x 72 DPI)

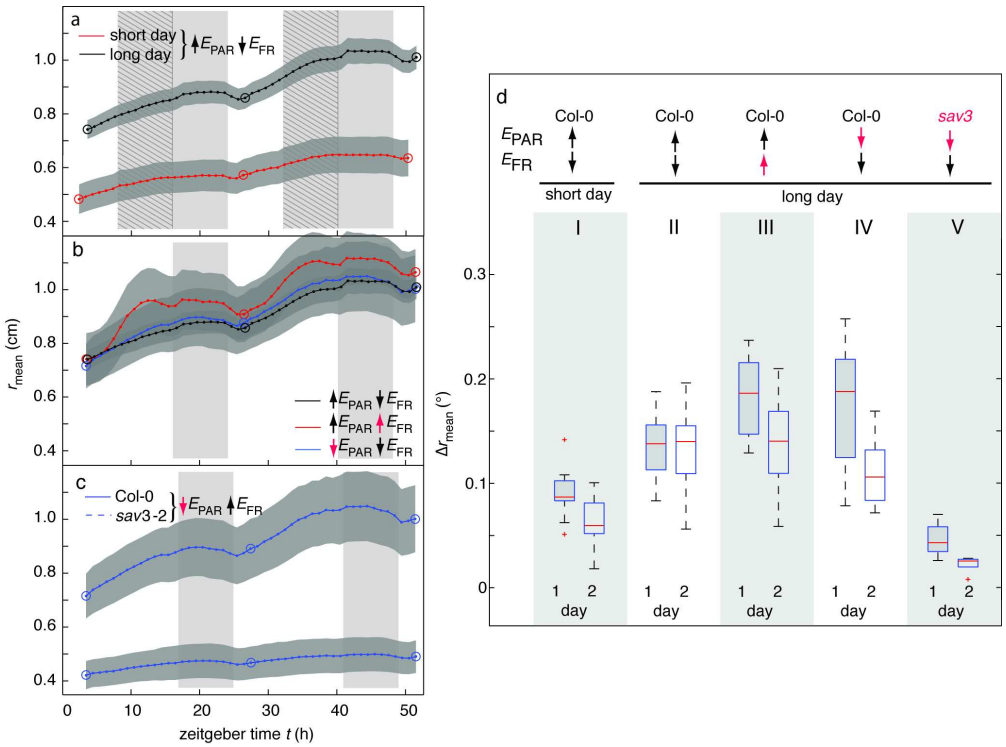

Fig. 6: (a-c) Diurnal pattern of rmean as a marker for the mean rosette radius or average leaf length of plants. Dots represent mean values for rmean computed from 15-30 individual plants. The grayish band around mean values for rmean represent the 95% confidence interval of mean estimate. Vertical gray boxes indicate the entrained night period in long day and the hatched part the supplemental night time in short day conditions. Plants were grown in a separate incubator at 21°C, EPAR=180 µmol m-2 s-1 and photoperiod for 15 days (long day) or 20 days (short day) prior to measurements. Specific treatments: (a) black: long day; red: short day; for both treatments: Col-0 at normal EPAR=150 µmol m-2 s-1 and normal EFR =4.5 µmol m-2 s-1; (b) black: normal EPAR=150 µmol m-2 s-1, EFR =4.5 µmol m-2 s-1; red: normal EPAR=150 µmol m-2 s-1 and supplemental EFR =22.5 µmol m-2 s-1; blue: reduced EPAR=39 µmol m-2 s-1; reduced EFR =1.5 µmol m-2 s-1); (c) solid line: Col-0; dashed line: sav3-2 mutant; reduced EPAR=39 µmol m-2 s-1; EFR =1.5 µmol m-2 s-1. (d) boxplots of the daily increase in rosette radius Δrmean measured for two consecutive days for different treatments presented in (a-c); from left to right: (I) Col-0, EPAR=150 µmol m-2, EFR =4.5 µmol m-2 s-1, short day; (II) Col-0, EPAR=150 µmol m-2, EFR =4.5 µmol m-2 s-1, long day, (III) Col-0, EPAR=150 µmol m-2, EFR =22.5 µmol m-2 s-1, long day; (IV) Col-0, EPAR=39 µmol m-2 s-1; EFR =1.5 µmol m-2 s-1, long day, (V) sav3-2 mutant; EPAR=39 µmol m-2 s-1; EFR =1.5 µmol m-2 s-1, long day.
726x538mm (72 x 72 DPI)